Published in final edited form as:
Dev Biol. 2007 July 1; 307(1): 43–52. doi:10.1016/j.ydbio.2007.04.005.

The transcription factor *Zfp423*/*OAZ* is required for cerebellar development and CNS midline patterning

Li Cheng and **Randall R. Reed**
Department of Molecular Biology and Genetics, Department of Neuroscience, Howard Hughes Medical Institute, Johns Hopkins University School of Medicine, 725 N Wolfe St, Baltimore, MD 21205

Abstract

The dorsal midline structure is critical for patterning the developing central nervous system (CNS). We show here that *Zfp423*/*OAZ*, a multiple zinc-finger transcription factor involved in both OE/EBF and BMP-signaling pathways, is required for the proper formation of forebrain and hindbrain midline structures. During embryogenesis, *OAZ* is highly expressed at the dorsal neuroepithelium flanking the roof-plate. *OAZ*-deficient mice are ataxic, attributed to the reduction of the cerebellar vermis and some regions of the hemispheres. Characterization of postnatal cerebellar development shows defects in Purkinje cell differentiation and granule cell proliferation. In the forebrain, dorsal telencephalic commissural neurons project axons, but these axons fail to cross the midline and midline glial cells are abnormally distributed. Moreover, there are malformations in midline structures including the septum, thalamus and hypothalamus, suggesting a pivotal role of OAZ in CNS midline patterning.

Keywords

midline; corpus callosum; cerebellum; ataxia; OAZ; zinc finger; transcription factor; BMP-signaling

Introduction

In the development of the vertebrate central nervous system (CNS), the dorsal midline of the neural tube acts as an important patterning center along the entire anterior-posterior axis (Chizhikov and Millen, 2005). The mechanisms of dorsal midline-dependent patterning are best studied in the developing spinal cord, in which roof-plate derived BMP and Wnt-signals control the specification, proliferation and differentiation of dorsal interneurons (Chizhikov and Millen, 2004; Helms and Johnson, 2003). Similarly, during cerebellar development, the isthmic organizer located at the dorsal mid-hindbrain junction establishes the cerebellar territory, and hindbrain roof-plate contributes to cell-type specification and proliferation (Alexandre and Wassef, 2003; Chizhikov et al., 2006; Louvi et al., 2003). The molecular mechanism underlying roof-plate dependent forebrain patterning is less understood. Evidence suggests that FGF and Wnt-signaling are involved in dorsal telencephalic patterning (Gunhaga et al., 2003; Storm et al., 2003), while BMP-signaling is required locally to pattern the dorsal midline itself (Hebert et al., 2002).

Correspondence: Randall R. Reed, Email: rreed@jhmi.edu, phone: 410-955-4631, fax: 410-955-0827.

Our genetic disruption studies implicate the transcription factor, *Zfp423*/*OAZ* (*OE*/*EBF* associated zinc-finger protein), in both forebrain and hindbrain midline structure formation. The OAZ protein, a 30 kruppel-like C_2H_2 type zinc-finger transcription factor, is involved in multiple signaling pathways via its multiple zinc-finger domains (Hata et al., 2000; Ku et al., 2006; Tsai and Reed, 1997; Tsai and Reed, 1998; Warming et al., 2004). OAZ was originally characterized in immature olfactory receptor neurons in which it negatively regulates transcription from mature olfactory-specific promoters (Tsai and Reed, 1997). Independent studies revealed that retroviral integration events that up-regulate OAZ, or the highly homologous gene Evi3, result in B-cell lymphomas (Warming et al., 2003; Warming et al., 2004). In both systems, OAZ may function as an inhibitor of OE/EBF proteins, a family of atypical helix-loop-helix transcription factors involved in various developmental processes including olfactory neuron maturation and B-cell differentiation (Lin and Grosschedl, 1995; Wang and Reed, 1993; Wang et al., 1997).

OAZ was also identified to be a downstream mediator of the BMP-signaling pathway (Hata et al., 2000; Ku et al., 2006; Ku et al., 2003; Shim et al., 2002). During early *Xenopus* development, OAZ interacts with Smad proteins after BMP stimulation and functions as a coactivator with Smads at BMP-regulated promoters *Xvent2* and *Xretpos* (Hata et al., 2000; Shim et al., 2002). OAZ also recruits Parp1, a chromatin-modifying enzyme, to the OAZ-Smads complex to cooperatively modulate BMP-target gene expression (Ku et al., 2003). Interestingly, Smad6, an inhibitor of the BMP pathway, is a mammalian target gene of OAZ (Ku et al., 2006). Taken together, tissue-specific OAZ expression may contribute to the intensity and duration of the BMP-signaling pathway.

Recent studies have demonstrated the specific contributions of OAZ to development of the cerebellum (Alcaraz et al., 2006; Warming et al., 2006). OAZ-deficient mice display specific defects in proliferation and differentiation of neural and glial precursors in the developing cerebellum especially near the midline (Alcaraz et al., 2006). In the present study, we have investigated OAZ expression during neuronal development and extended the loss-of-function analysis of OAZ to the entire brain by immunostaining and micro-diffusion tensor imaging (μDTI). OAZ is highly expressed in the developing dorsal neuroepithelium flanking the roof-plate and OAZ deletion in mice impairs both forebrain and hindbrain midline structures. In *OAZ*-null mice, an early fusion defect in the hindbrain results in loss of the cerebellar vermis and part of the hemispheres. During postnatal cerebellar development, Purkinje cell (PC) differentiation and granule cell (GC) proliferation are affected. In the forebrain, OAZ deletion causes anomalies in the septum, thalamus and hypothalamus. In addition, major commissural tracks including the corpus callosum and hippocampal commissure fail to cross the midline as a result of earlier midline patterning defects. These experiments provide *in vivo* evidence for the multi-functional nature of this transcription factor and underscore the importance of OAZ-mediated signaling in CNS midline patterning.

Materials and Methods

Mouse Genetics

The OAZ^{lacZ} mouse line was generated from ES cell line XB409 (Bay Genomics - baygenomics.ucsf.edu) by blastocyst injection. The exact insertion site was mapped by Southern blot analysis and specific PCR primers were designed for genotyping (wild-type allele: forward primer, 5′-CTGGATCAGCCCTTCTTGAGTCCTA-3′; reverse primer, 5′-CAATGGCGAGGAAGAAACTCTGATG-3′; tagged allele: the forward primer paired with a third primer in the lacZ gene 5′-CCACAACGGGTTCTTCTGTTAGTCC-3′). The *OAZ* knock-out targeting vector was constructed from restriction fragments of 6kb and 5kb flanking exon 4 of the SVJ129 *OAZ* gene. An *IRES-YFP-pA* cassette followed by the *LoxP-TK(Δ)-Neo-LoxP (LTNL)* cassette was inserted at amino acid 112 and replaced the downstream sequence

in exon 4. Homologous integrants were identified by Southern blot and correctly targeted ES cells were injected into C57BL/6 blastocysts. The F1 heterozygous mice were mated with Cre-expressing transgenic mice to remove the *LTNL* cassette. Mice were genotyped using a 3-primer PCR analysis of genomic DNA, with forward and reverse primers amplifying the wild-type allele (forward primer, 5′-GTGCCTCAAAGAGTTCCGTAGCAAG-3′; reverse primer, 5′-AGTGCTGCCTCTCTGGGTTGCGATA-3′), and a third primer in the YFP sequence (forward primer, 5′-CTTCTTCAAGGACGACGGCAACTA-3′). The *OAZ* wild-type allele is detected as a ~410bp product and the targeted allele as a ~820bp product. All mice were maintained on a mixed 129/BL6 background.

X-gal Staining, Immunolocalization and In situ hybridization

X-gal whole-mount and section staining were performed as described (Monuki et al., 2001). Immunohistochemistry was performed on paraffin or PFA sections. The following primary antibodies were used: BrdU (rat, 1:100; Abcam, Cambridge MA), GFAP (rabbit, 1:1000, Sigma, St. Louis MO), parvalbumin (mouse, 1: 2000; Sigma), neurofilament M (rabbit, 1:1000, Chemicon, Temecula, CA) and Zic1 (rabbit, 1:400; Rockland, Philadelphia, PA). Alexa 546-labeled secondary antibodies were used at 1:1000 dilutions. Biotinylated secondary antibodies were used at 1:200 dilutions and detected with streptavidin-conjugated peroxidase (Vector Labs, Burlingame, CA). DAPI was used as a nuclear counterstain in fluorescent images. *In situ* hybridization with the *OAZ* probe (NM_033327, nucleotide 102–1715) was performed on PFA-fixed sections following a standard protocol (Wang et al., 2004). Images were obtained with either a Leica stereomicroscope or a Zeiss Axioplan microscope except Zic1 staining was obtained with a Zeiss LSM 510 confocal laser-scanning microscope.

BrdU Labeling and counting

Pregnant females or pups were injected intraperitoneally with BrdU (Sigma) 50μg/g body weight 30 min before they were sacrificed. Sections were incubated with 3N HCl for 30min before immunostaining with anti-BrdU antibody. Counting of BrdU+ cells was performed on images taken at 10× magnification. *MRI*. P0 $OAZ^{-/-}$ and $OAZ^{+/-}$ heads were immersion-fixed in 4%PFA. P20 mice were perfused with 4% PFA and the brains were removed from skull and post-fixed in 4% PFA until imaged. Imaging was performed as previously described (Wang et al., 2006).

Results

OAZ expression assayed with a *β-geo* gene-trap reporter

To define OAZ expression, we generated genetically modified mice from an ES cell line (XB409) harboring a *β-geo* gene-trap reporter into the last intron of *OAZ* gene. This insertion resulted in the deletion of nine amino acids from the C-terminus of OAZ and expression of an OAZ-β-geo fusion protein (Fig. 1a). At embryonic (E) 8.5, $OAZ^{lacZ/+}$ mice display bilateral expression of the OAZ-β-geo reporter along the dorsal neural tube (Fig. 1b) and this expression continued through later embryonic stages. At E9.5, OAZ was expressed as two narrow continuous bands along the dorsal midline extending from the telencephalon caudally along the entire body axis (Fig. 1c, d). In transverse sections, OAZ expression was mainly detected in the neuroepithelum, with the most intense staining at the dorsal region flanking the roof-plate (Fig. 1e–g). Later in embryonic development, X-gal staining was detected in limbs, lung, and the cranial sensory placodes, including the olfactory, lens, otic placodes and branchial arches (data not shown). In sagittal sections of E14.5 $OAZ^{lacZ/+}$ embryo, strong X-gal staining was detected in the olfactory epithelium, thalamus, septum, midbrain ventricular zone and the cerebellar primordium (Fig. 1h). Weak X-gal staining was also detected in the cortical ventricular zone at this stage.

In the developing cerebellar primordia, OAZ expression was detected in the Purkinje cell (PC) layer and the external granular layer (EGL) (Fig. 1i). The staining at both the PC and EGL decreased postnatally (Fig. 1j, k) and is absent in adulthood. Interestingly, higher levels of OAZ expression were observed in the rostral lobes than in caudal lobes of the PC layer (Fig. 1j, k).

We verified that the reporter expression mimicked the endogenous OAZ expression by *in situ* hybridization. The sites of specific OAZ *in situ* signal (Fig. 2a, d, g) reflect those regions displaying X-gal staining in $OAZ^{lacZ/+}$ mice (Fig. 2b, e, h), confirming that the OAZ-lacZ reporter faithfully mimics the pattern of endogenous OAZ expression.

Early midline defects in homozygous $OAZ^{lacZ/lacZ}$ reporter mice

Heterozygous $OAZ^{lacZ/+}$ mice were indistinguishable from their wild-type littermates in terms of viability, growth, appearance and fertility. In contrast, $OAZ^{lacZ/lacZ}$ pups were smaller than littermates and died within one day of birth except two (from 31 litters) survived to three weeks (Table 1). Examination of $OAZ^{lacZ/lacZ}$ embryos revealed striking morphological defects in the forebrain and hindbrain. The most obvious anomalies related to midline structures and enlarged ventricles (Fig. 2c, f, i). In E15.5 $OAZ^{lacZ/lacZ}$ embryos, the septum was reduced, and the interventricular foramen that connects the lateral ventricles with the third ventricle was enlarged, manifested as a gap in the ventral midline area at the forebrain (Fig. 2c, indicated by "*"). At the hindbrain, the cerebellar plate and the medulla oblongata were considerably smaller, while the fourth ventricle was enlarged (Fig. 2i). Taken together, these results indicate that OAZ contributes to the morphogenesis of CNS midline structures.

Targeted deletion of *OAZ*

The defects observed in $OAZ^{lacZ/lacZ}$ mice could arise from loss-of-function of endogenous OAZ, or alternatively, by aberrant OAZ function as a result of fusion with β-geo protein. To address this point, we designed a targeted deletion of the *OAZ* gene by inserting an *IRES-YFP*-polyA reporter at amino acid 112 to replace exon 4 and eliminate the remainder of the OAZ open reading frame. The truncated OAZ protein, even if stable, would lack 91% (1180/1292) of the OAZ protein including all the known DNA-binding and protein-binding domains. This presumptive functional null allele is hereafter referred to as OAZ^{-} (Fig. 3a). Homozygous $OAZ^{-/-}$ progeny were obtained at the expected Mendelian ratio and more than half of the $OAZ^{-/-}$ pups (16% of total progeny) survived to three weeks (Table 1). During postnatal development, $OAZ^{-/-}$ survivors were ataxic, weighed considerably less than wild-type and heterozygous littermates (weight at P20: control, 11.6±1.5g, n=15; $OAZ^{-/-}$, 4.9±1.2g, n=15, $P<0.001$) and died by approximately four weeks. We examined the $OAZ^{-/-}$ mice at P20-P25 unless otherwise specified. Gross anatomic examination of the brain showed defects in the cerebellum, forebrain and olfactory bulb.

Cerebellar defects in *OAZ*-tagged mice and $OAZ^{-/-}$ mice

The adult $OAZ^{-/-}$ mice and the few $OAZ^{lacZ/lacZ}$ survivors exhibited severe ataxia. Most were unable to maintain their balance and showed poorly coordinated movement, indicating cerebellar anomalies (Supplemental video 1). Morphological examination of $OAZ^{-/-}$ brains revealed that the lateral cerebellar hemispheres were smaller with fewer folia and the central vermis region was severely reduced (Fig. 3c) or in some cases even failed to form (Fig. 3d). Analysis of serial coronal sections through the cerebellum confirmed the reduction of the hemispheres and the vermis (Fig. 3e, f). The only place where cerebellar tissue was observed was adjacent to the midbrain. In the most severely affected mice, the entire cerebellum was absent (Fig. 3d).

We examined the postnatal cerebellar growth in sagittal sections. Differentiation of PCs was examined by immunostaining for parvalbumin, a gene highly expressed in PCs and associated with neuronal differentiation (Jankowski et al., 2004). The P3 *OAZ*$^{-/-}$ cerebella were smaller in size and lacked foliation compared with wild-type controls (Fig. 4a, b). At P10 (Fig. 4c, d) and adulthood, the number and dendritic arborization of PCs were greatly reduced in *OAZ*$^{-/-}$ mice. Despite these morphological defects, the laminar arrangement of cells in the cerebellar cortex was maintained.

During postnatal cerebellar development, GC progenitors located at the EGL exit the cell cycle and migrate inwardly to the internal granular layer (IGL). To examine GC proliferation, we performed BrdU pulse-injection in *OAZ*$^{-/-}$ mice and wild-type littermates at different ages. In wild-type control mice, extensive proliferation at the EGL could be observed at P3 and P7, which then greatly decreased to a single cell layer at P10 (Fig. 4e, g). In *OAZ*$^{-/-}$ mice, the number of BrdU-positive cells was reduced at P3 and P7 compared with wild-type mice, but was relatively increased at P10 (Fig. 4f, h, k), suggesting that the peak of GC proliferation was delayed.

Despite the delay and reduction of proliferation, the differentiation and migration of GCs could proceed grossly normally and mature GCs, stained by GC marker *Zic1* (Lewis et al., 2004), can be detected at the IGL in adult *OAZ*$^{-/-}$ mice (Fig. 4i, j). Taken together, these experiments show that *OAZ*-deletion impairs postnatal cerebellum development including folia formation, PC differentiation and GC proliferation.

OAZ loss-of-function disrupts cerebellar vermis development

The cerebellum is formed from two bilateral primordia that fuse in the dorsal midline while the vermis arises from the medial region where the fusion occurs (Alexandre and Wassef, 2003; Louvi et al., 2003). We examined the developing cerebellum at E13.5, when fusion initiates. In *OAZ*$^{-/-}$ embryos, the cerebellar primordia were considerably smaller (Fig. 5a, b). When we examined cell proliferation by BrdU labeling, there were similar patterns of proliferating cells at the cerebellar ventricular zone (Fig. 5a, b, e). At E15.5, the two primordia extended posteriorly and fused across the dorsal midline to form a tube-like cerebellar plate in wild-type mice (Fig. 5c, dashed line). In *OAZ*$^{-/-}$ mice, however, the two primordia were barely attached at the medial region, which failed to further expand. In addition, the medulla oblongata and rostral spinal cord remained open in *OAZ*$^{-/-}$ mice (Fig. 5d, arrows). Similar defects were observed in embryos and neonates of *OAZ*$^{lacZ/lacZ}$ mice (Fig. 2i and data not shown). Together, these experiments suggest that OAZ is involved in cerebellar development, in particular the formation of the vermis region.

Forebrain midline defects in *OAZ*$^{-/-}$ mice

OAZ is highly expressed in the forebrain neuroepithelium (Fig. 1d) and *OAZ*$^{lacZ/lacZ}$ embryos exhibit major defects in the forebrain septal region (Fig. 2c). Early midline patterning is critical for subsequent developmental events, including crossing of commissural axons at the midline (Richards et al., 2004). We examined the formation of three major forebrain commissural axon tracts in *OAZ*$^{-/-}$ mice: the corpus callosum, the hippocampal commissure and the anterior commissure. In P0 (Fig. 6a–d) and adult *OAZ*$^{-/-}$ mice, we observed defects in the formation of corpus callosum and hippocampal commissure, through which the cortical and hippocampal neurons project to the opposite hemisphere. In *OAZ*$^{-/-}$ mice, callosal axons projected normally along the intermediate zone of the cortical plate, but when they approached the midline, they failed to cross the midline. Instead, axons swirled into longitudinal neuromas called Probst bundles (Fig. 6b), structures typically observed in callosal agenesis that results from defects in midline fusion or abnormal midline signaling (Richards et al., 2004). In addition, *OAZ*$^{-/-}$

mice frequently possessed enlarged cerebral ventricles accompanied with shrinkage of the thalamus (Fig. 6d).

Similar to $OAZ^{lacZ/lacZ}$ mice, analysis of $OAZ^{-/-}$ embryos revealed a defect in the formation of the septum (Fig. 6f, h, indicated by "*"), which could contribute to the subsequent defects of commissural axon crossing at the midline. The pattern of BrdU pulse-labeled cells located at the cortical ventricular surface appeared normal in $OAZ^{-/-}$ mice, suggesting that the defects of commissural axon crossing are likely to arise from abnormal midline patterning instead of proliferation defects of cortical neurons. In particular, midline glial cells are thought to play critical roles in guiding commissural axons crossing at the midline (Shu and Richards, 2001). We examined the presence of midline glia using an anti-GFAP antibody (Tole et al., 2006). At E15.5, GFAP staining marked the midline glia as a continuous cell stream connecting the two cortical hemispheres at the corticoseptal boundary in control mice (Fig. 6i). In $OAZ^{-/-}$ mice, GFAP staining was preserved at the cortical edge (Fig. 6j, arrows), but not in the medial region through which callosal axons cross. These experiments indicate that OAZ is important for early forebrain midline patterning and the subsequent crossing of commissural tracts at the midline.

μ DTI imaging revealed widespread midline defects in $OAZ^{-/-}$ mice

To systematically survey the $OAZ^{-/-}$ brain, we analyzed $OAZ^{-/-}$ and wild-type brain using magnetic resonance diffusion tensor imaging (μDTI), which reveals the location and orientation of axon tracts in the brain (Jacobs et al., 1999; Mori et al., 2001; Wang et al., 2006). Serial μDTI images of P0 and P20 $OAZ^{-/-}$ and wild-type brains were processed for three-dimensional reconstruction and examined in different planes. In the midsagittal plane, the $OAZ^{-/-}$ brains lack the two dorsal commissural tracts, the corpus callosum and hippocampal commissure. The ventral commissural tract, the anterior commissure, was present but smaller (Fig. 7a, b). In coronal planes, the failure of callosal and hippocampal axon crossing at the midline and the anomalies in the septal region were apparent (Fig. 7c, d). Additionally, both the cerebral peduncle and fasciculus retroflexus occupied a larger area in the P0 $OAZ^{-/-}$ brain, and the anterior hypothalamus was smaller (Fig. 7f). A complete animated series of coronal and horizontal images of P20 $OAZ^{-/-}$ and wild-type mice are provided online (see Supplemental figures 2–5). Confirming and extending the histological staining data, the μDTI imaging experiments revealed widespread CNS midline defects in $OAZ^{-/-}$ mice.

Discussion

The OAZ protein participates in multiple signaling pathways by utilizing different clusters of zinc-finger domains to modulate OE/EBF transcription factor activity and BMP signaling. Our current studies show that OAZ is expressed at the dorsal neuroepithelium flanking the roof plate during embryonic development, and OAZ-deletion affects both forebrain and hindbrain midline patterning.

It is remarkable that neonatal lethality is almost always observed in the $OAZ^{lacZ/lacZ}$ mice given that only nine amino acids were deleted from the 1292-aa protein. Although it is tempting to speculate that the last zinc finger (aa1269—aa1289), critical for the association of OAZ with OE/EBF proteins (Tsai and Reed, 1998), underlies this lethality, it equally possible that the fusion of β-geo reporter to the C-terminus prevents nuclear localization and functions as a partial dominant-negative by sequestering interacting proteins outside of the nucleus. This model would explain the significantly greater lethality observed in $OAZ^{lacZ/lacZ}$ mice than in $OAZ^{-/-}$ mice. The null allele generated by Warming et al displays a similar viability (Warming et al., 2006). The compound heterozygous progeny ($OAZ^{lacZ/-}$) from crossing heterozygous knock-out mice ($OAZ^{+/-}$) and heterozygous gene-trap mice ($OAZ^{lacZ/+}$) also show a high neonatal lethality similar to that observed in $OAZ^{lacZ/lacZ}$ mice (Table 1), implicating that this gene trap allele is a dominant allele and may disrupt interactions between OAZ and other

proteins. Specifically, the highly related protein Evi3 is coexpressed with OAZ in many tissues (Warming et al., 2003) and can regulate both OE/EBF-dependent and BMP-dependent transcriptional activations (Bond et al., 2004).

One *OAZ* gene-trap line (XH542), harboring a β-geo vector insertion into *OAZ* intron 3, was reported to be a hypomorphic allele leading to mild cerebellar hypoplasia in compound heterozygous animals (*XH542*/*null* mice) (Alcaraz et al., 2006; Warming et al., 2006). Interestingly, the XB409 allele characterized here with a gene trap insertion into a more distal position (intron 7) completely recapitulates the phenotype observed in *OAZ*-null allele. The difference observed with these two gene-trap alleles may result from alternative splicing of OAZ. The ability of the OAZ protein to engage multiple pathways, each mediated by distinct Zn^{2+} finger clusters, suggests that complex phenotypes might arise in gene-trap alleles that retain different regions of the native protein. The elimination of all of the recognized functional domains in the YFP-tagged *null*-allele described here and the untagged *null*-alleles (Alcaraz et al., 2006; Warming et al., 2006) provide tools for future studies.

We examined cerebellar development in $OAZ^{-/-}$ mice at both the morphological level and the cellular level. The earliest morphological difference is observed at E13.5, when the cerebellar primordia appeared smaller in $OAZ^{-/-}$ mice. The cerebellar vermis, which arise from the medial region where two lateral primordia fuse, seems to be particularly sensitive to OAZ loss-of-function. As a result, little or no vermis region is present in adult $OAZ^{-/-}$ mice. Additionally, we characterized PC differentiation and GC proliferation in postnatal development and showed both processes were disturbed in $OAZ^{-/-}$ mice. Alcarez et al have reported specific defects in GC proliferation near the cerebellar midline at embryonic ages and documented abnormal differentiation and migration of glial cells in this region (Alcaraz et al., 2006).

Mutations affecting the isthmus organizer at the mid-hindbrain boundary and/or hindbrain roof plate often result in a similar phenotype as in $OAZ^{-/-}$ mice in that the cerebellar vermis and part of the hemispheres are deleted (Broccoli et al., 1999; Li et al., 2002; Millonig et al., 2000; Thomas et al., 1991; Wurst et al., 1994). In the spontaneous mouse mutant *dreher*, which harbors mutations in the *Lmx1* gene, the cerebellar vermis is greatly reduced (Manzanares et al., 2000; Millonig et al., 2000). Analysis of *dreher* embryos revealed that the roof plate adjacent to the cerebellar territory is severely reduced. In particular, the Bmp6-expressing cells at the dorsal roof-plate were absent, suggesting that roof-plate derived BMP-signaling is required for cerebellar vermis formation (Millonig et al., 2000). In addition, fate-mapping experiments in chick embryos showed that the paramedial isthmic neuroepithelium participates in the formation of cerebellar vermis, and BMP-signaling may be involved in this process (Louvi et al., 2003). In our current study, we have shown that the Smad cofactor OAZ is expressed at the dorsal neuroepithelium flanking the roof plate. During embryogenesis, there are defects relating to midline structures in $OAZ^{lacZ/lacZ}$ and $OAZ^{-/-}$ mice. Further examination of the expression pattern of midline markers, especially components in the BMP-signaling pathway, is necessary to directly elucidate the mechanisms by which OAZ regulates midline formation. Nevertheless, our data supports a role for OAZ-mediated BMP-signaling in CNS pattern formation.

BMP-signaling also plays a role in cell specification in the developing cerebellum. Bmp6/7 and Gdf7 are sufficient to initiate the program of GC specification in explant cultures (Alder et al., 1999). In addition, double knock-out of the type I BMP receptor genes *Bmpr1a* and *Bmpr1b* in mice leads to a dramatic reduction of GCs (Qin et al., 2006). OAZ expression is detected at both the PC layer and EGL in the developing cerebellum and the expression is diminished in adult mice, indicating that OAZ plays a role in cell proliferation/differentiation during cerebellar development. In $OAZ^{-/-}$ mice, the differentiation of PC is disturbed. The number of PCs is greatly reduced and the remaining PCs show poorly differentiated dendrites.

Interestingly, an OAZ-interacting protein OE3/EBF2 has been shown to be expressed in PCs and contribute to PC migration and cerebellar cortical topography (Croci et al., 2006). It seems likely that the action of OAZ in multiple pathways, including tissue patterning and cellular differentiation, may underlie the cerebellar anomalies observed in *OAZ*$^{-/-}$ mice.

Here we have demonstrated a specific role of OAZ in forebrain development. The OAZ gene is expressed in midline structures, including the septum, thalamus and hypothalamus and loss of OAZ function causes anomalies in these structures. Crossing of the corpus callosum and hippocampal commissure at the midline is also disrupted. As both anti-neurofilament staining and μDTI imaging showed that these axons make normal initial projections in *OAZ*$^{-/-}$ mice, the midline crossing defects are not due to a loss of the contralaterally projecting neurons or defects in axonal outgrowth. GFAP staining reveals that the distribution of midline glia cells is disrupted, which may underlie the failure of midline crossing. Our results on developmental defects in *OAZ*$^{-/-}$ mice in forebrain and hindbrain structures and related studies specifically focused on cerebellar development (Alcaraz et al., 2006; Warming et al., 2006) suggest an important function for OAZ in midline structures along the entire rostral-caudal axis.

The widespread forebrain defects relating to midline structures in *OAZ*$^{-/-}$ mice underscore the potential importance of BMP-signaling in forebrain patterning. Multiple BMPs are expressed at high levels in the forebrain roof-plate (Chizhikov and Millen, 2005), and exogenous Bmp4 and Bmp5 can induce forebrain patterning defects, including holoprosencephaly (a single cerebral hemisphere), cyclopia (a single midline eye), and loss of ventral midline structures (Golden et al., 1999). In addition, Gdf7-mediated roof-plate ablation leads to failure of midline induction and holoprosencephaly in mice, while exogenous Bmp4 is sufficient to rescue the midline patterning defects in explant cultures (Cheng et al., 2006). It has been proposed that the tissue-specific OAZ expression may contribute to the intensity and duration of the BMP-signaling pathway (Ku et al., 2006). The specific expression of OAZ in the dorsal midline adjacent to the roof-plate and the midline-related defects from loss-of-function of OAZ support the role of roof-plate directed BMP-signaling in CNS pattern formation.

S1. Video of a P20 wild-type and two OAZ$^{-/-}$ mice. The two smaller animals (OAZ$^{-/-}$ animals) display severe ataxia.

Supplemental Figures 2–5 Reconstructed μDTI images of brains from wild-type (Fig. S2 - coronal plane, Fig. S4 -horizontal plane) and OAZ$^{-/-}$ mice (Fig. S3 - coronal plane, Fig. S5 – horizontal plane) at P20.

Supplementary Material

Refer to Web version on PubMed Central for supplementary material.

Acknowledgments

We thank Dr. J. Zhang and Dr. S. Mori for the MRI imaging study (Johns Hopkins University, MRI center) and Dr. Yanshu Wang for her guidance on paraffin tissue preparation. We appreciate the insightful suggestions from Dr. Yulan Cheng and Dr. Alex Joyner. We thank members of the Reed lab and Dr. J. Nathans for helpful discussions.

References

Alcaraz WA, Gold DA, Raponi E, Gent PM, Concepcion D, Hamilton BA. Zfp423 controls proliferation and differentiation of neural precursors in cerebellar vermis formation. Proc Natl Acad Sci U S A. 2006

Alder J, Lee KJ, Jessell TM, Hatten ME. Generation of cerebellar granule neurons in vivo by transplantation of BMP-treated neural progenitor cells. Nat Neurosci 1999;2:535–40. [PubMed: 10448218]

Alexandre P, Wassef M. The isthmic organizer links anteroposterior and dorsoventral patterning in the mid/hindbrain by generating roof plate structures. Development 2003;130:5331–8. [PubMed: 14507781]

Bond HM, Mesuraca M, Carbone E, Bonelli P, Agosti V, Amodio N, De Rosa G, Di Nicola M, Gianni AM, Moore MA, Hata A, Grieco M, Morrone G, Venuta S. Early hematopoietic zinc finger protein (EHZF), the human homolog to mouse Evi3, is highly expressed in primitive human hematopoietic cells. Blood 2004;103:2062–70. [PubMed: 14630787]

Broccoli V, Boncinelli E, Wurst W. The caudal limit of Otx2 expression positions the isthmic organizer. Nature 1999;401:164–8. [PubMed: 10490025]

Cheng X, Hsu CM, Currle DS, Hu JS, Barkovich AJ, Monuki ES. Central roles of the roof plate in telencephalic development and holoprosencephaly. J Neurosci 2006;26:7640–9. [PubMed: 16855091]

Chizhikov VV, Lindgren AG, Currle DS, Rose MF, Monuki ES, Millen KJ. The roof plate regulates cerebellar cell-type specification and proliferation. Development 2006;133:2793–804. [PubMed: 16790481]

Chizhikov VV, Millen KJ. Mechanisms of roof plate formation in the vertebrate CNS. Nat Rev Neurosci 2004;5:808–12. [PubMed: 15378040]

Chizhikov VV, Millen KJ. Roof plate-dependent patterning of the vertebrate dorsal central nervous system. Dev Biol 2005;277:287–95. [PubMed: 15617675]

Croci L, Chung SH, Masserdotti G, Gianola S, Bizzoca A, Gennarini G, Corradi A, Rossi F, Hawkes R, Consalez GG. A key role for the HLH transcription factor EBF2COE2,O/E-3 in Purkinje neuron migration and cerebellar cortical topography. Development 2006;133:2719–29. [PubMed: 16774995]

Golden JA, Bracilovic A, McFadden KA, Beesley JS, Rubenstein JL, Grinspan JB. Ectopic bone morphogenetic proteins 5 and 4 in the chicken forebrain lead to cyclopia and holoprosencephaly. Proc Natl Acad Sci U S A 1999;96:2439–44. [PubMed: 10051661]

Gunhaga L, Marklund M, Sjodal M, Hsieh JC, Jessell TM, Edlund T. Specification of dorsal telencephalic character by sequential Wnt and FGF signaling. Nat Neurosci 2003;6:701–7. [PubMed: 12766771]

Hata A, Seoane J, Lagna G, Montalvo E, Hemmati-Brivanlou A, Massague J. OAZ uses distinct DNA- and protein-binding zinc fingers in separate BMP-Smad and Olf signaling pathways. Cell 2000;100:229–40. [PubMed: 10660046]

Hebert JM, Mishina Y, McConnell SK. BMP signaling is required locally to pattern the dorsal telencephalic midline. Neuron 2002;35:1029–41. [PubMed: 12354394]

Helms AW, Johnson JE. Specification of dorsal spinal cord interneurons. Curr Opin Neurobiol 2003;13:42–9. [PubMed: 12593981]

Jacobs RE, Ahrens ET, Meade TJ, Fraser SE. Looking deeper into vertebrate development. Trends Cell Biol 1999;9:73–6. [PubMed: 10087623]

Jankowski J, Holst MI, Liebig C, Oberdick J, Baader SL. Engrailed-2 negatively regulates the onset of perinatal Purkinje cell differentiation. J Comp Neurol 2004;472:87–99. [PubMed: 15024754]

Ku M, Howard S, Ni W, Lagna G, Hata A. OAZ Regulates Bone Morphogenetic Protein Signaling through Smad6 Activation. J Biol Chem 2006;281:5277–87. [PubMed: 16373339]

Ku MC, Stewart S, Hata A. Poly(ADP-ribose) polymerase 1 interacts with OAZ and regulates BMP-target genes. Biochem Biophys Res Commun 2003;311:702–7. [PubMed: 14623329]

Lewis PM, Gritli-Linde A, Smeyne R, Kottmann A, McMahon AP. Sonic hedgehog signaling is required for expansion of granule neuron precursors and patterning of the mouse cerebellum. Dev Biol 2004;270:393–410. [PubMed: 15183722]

Li JY, Lao Z, Joyner AL. Changing requirements for Gbx2 in development of the cerebellum and maintenance of the mid/hindbrain organizer. Neuron 2002;36:31–43. [PubMed: 12367504]

Lin H, Grosschedl R. Failure of B-cell differentiation in mice lacking the transcription factor EBF. Nature 1995;376:263–7. [PubMed: 7542362]

Louvi A, Alexandre P, Metin C, Wurst W, Wassef M. The isthmic neuroepithelium is essential for cerebellar midline fusion. Development 2003;130:5319–30. [PubMed: 14507778]

Manzanares M, Trainor PA, Ariza-McNaughton L, Nonchev S, Krumlauf R. Dorsal patterning defects in the hindbrain, roof plate and skeleton in the dreher (dr(J)) mouse mutant. Mech Dev 2000;94:147–56. [PubMed: 10842066]

Millonig JH, Millen KJ, Hatten ME. The mouse Dreher gene Lmx1a controls formation of the roof plate in the vertebrate CNS. Nature 2000;403:764–9. [PubMed: 10693804]

Monuki ES, Porter FD, Walsh CA. Patterning of the dorsal telencephalon and cerebral cortex by a roof plate-Lhx2 pathway. Neuron 2001;32:591–604. [PubMed: 11719201]

Mori S, Itoh R, Zhang J, Kaufmann WE, van Zijl PC, Solaiyappan M, Yarowsky P. Diffusion tensor imaging of the developing mouse brain. Magn Reson Med 2001;46:18–23. [PubMed: 11443706]

Qin L, Wine-Lee L, Ahn KJ, Crenshaw EB 3rd. Genetic analyses demonstrate that bone morphogenetic protein signaling is required for embryonic cerebellar development. J Neurosci 2006;26:1896–905. [PubMed: 16481421]

Richards LJ, Plachez C, Ren T. Mechanisms regulating the development of the corpus callosum and its agenesis in mouse and human. Clin Genet 2004;66:276–89. [PubMed: 15355427]

Shim S, Bae N, Han JK. Bone morphogenetic protein-4-induced activation of Xretpos is mediated by Smads and Olf-1/EBF associated zinc finger (OAZ). Nucleic Acids Res 2002;30:3107–17. [PubMed: 12136093]

Shu T, Richards LJ. Cortical axon guidance by the glial wedge during the development of the corpus callosum. J Neurosci 2001;21:2749–58. [PubMed: 11306627]

Storm EE, Rubenstein JL, Martin GR. Dosage of Fgf8 determines whether cell survival is positively or negatively regulated in the developing forebrain. Proc Natl Acad Sci U S A 2003;100:1757–62. [PubMed: 12574514]

Thomas KR, Musci TS, Neumann PE, Capecchi MR. Swaying is a mutant allele of the proto-oncogene Wnt-1. Cell 1991;67:969–76. [PubMed: 1835670]

Tole S, Gutin G, Bhatnagar L, Remedios R, Hebert JM. Development of midline cell types and commissural axon tracts requires Fgfr1 in the cerebrum. Dev Biol 2006;289:141–51. [PubMed: 16309667]

Tsai RY, Reed RR. Cloning and functional characterization of Roaz, a zinc finger protein that interacts with O/E-1 to regulate gene expression: implications for olfactory neuronal development. J Neurosci 1997;17:4159–69. [PubMed: 9151733]

Tsai RY, Reed RR. Identification of DNA recognition sequences and protein interaction domains of the multiple-Zn-finger protein Roaz. Mol Cell Biol 1998;18:6447–56. [PubMed: 9774661]

Wang MM, Reed RR. Molecular cloning of the olfactory neuronal transcription factor Olf-1 by genetic selection in yeast. Nature 1993;364:121–6. [PubMed: 8321284]

Wang SS, Lewcock JW, Feinstein P, Mombaerts P, Reed RR. Genetic disruptions of O/E2 and O/E3 genes reveal involvement in olfactory receptor neuron projection. Development 2004;131:1377–88. [PubMed: 14993187]

Wang SS, Tsai RY, Reed RR. The characterization of the Olf-1/EBF-like HLH transcription factor family: implications in olfactory gene regulation and neuronal development. J Neurosci 1997;17:4149–58. [PubMed: 9151732]

Wang Y, Zhang J, Mori S, Nathans J. Axonal growth and guidance defects in Frizzled3 knock-out mice: a comparison of diffusion tensor magnetic resonance imaging, neurofilament staining, and genetically directed cell labeling. J Neurosci 2006;26:355–64. [PubMed: 16407530]

Warming S, Liu P, Suzuki T, Akagi K, Lindtner S, Pavlakis GN, Jenkins NA, Copeland NG. Evi3, a common retroviral integration site in murine B-cell lymphoma, encodes an EBFAZ-related Kruppel-like zinc finger protein. Blood 2003;101:1934–40. [PubMed: 12393497]

Warming S, Rachel RA, Jenkins NA, Copeland NG. Zfp423 is required for normal cerebellar development. Mol Cell Biol 2006;26:6913–22. [PubMed: 16943432]

Warming S, Suzuki T, Yamaguchi TP, Jenkins NA, Copeland NG. Early B-cell factor-associated zinc-finger gene is a frequent target of retroviral integration in murine B-cell lymphomas. Oncogene 2004;23:2727–31. [PubMed: 15048087]

Wurst W, Auerbach AB, Joyner AL. Multiple developmental defects in Engrailed-1 mutant mice: an early mid-hindbrain deletion and patterning defects in forelimbs and sternum. Development 1994;120:2065–75. [PubMed: 7925010]

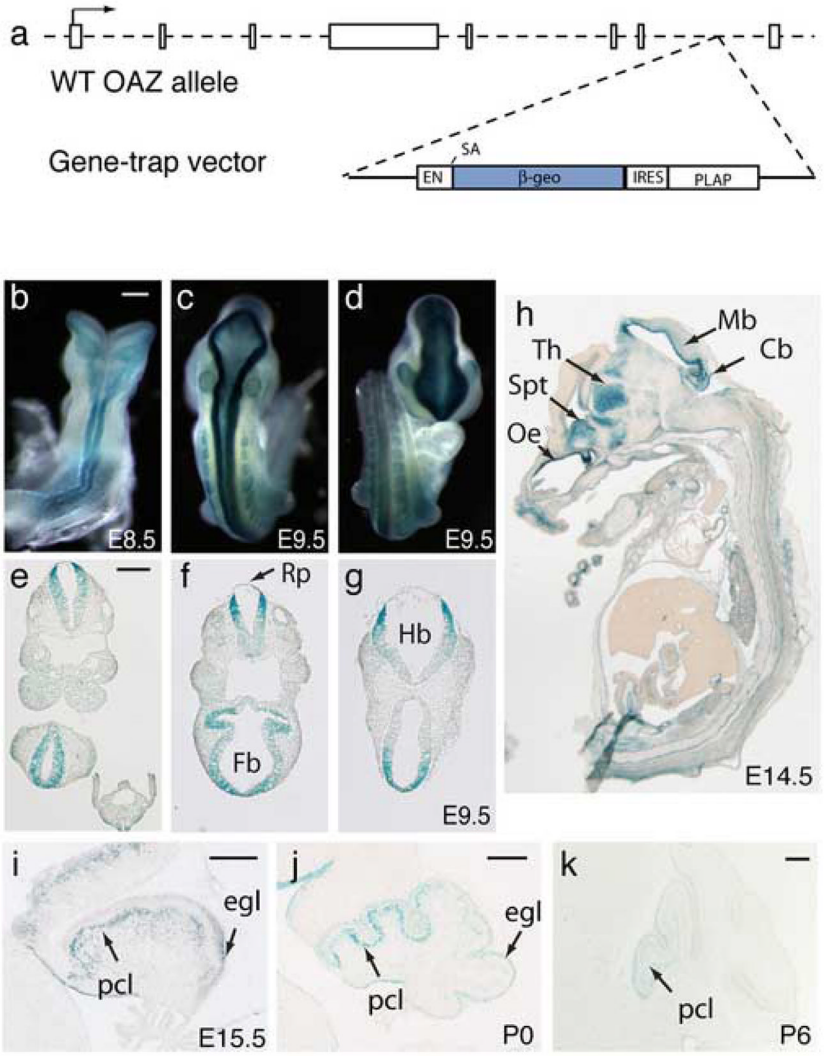

Figure 1.

OAZ expression pattern assayed with a β-geo gene-trap reporter in mice

(a) Schematic representation of the *OAZ* gene-trap allele XB409. The gene-trap vector was inserted in the last intron of *OAZ*, resulting in the expression of an OAZ-β-geo fusion protein and the deletion of nine amino acids from the C-terminus of OAZ. (b–d) Whole-mount X-gal staining of $OAZ^{lacZ/+}$ embryos. Expression of the OAZ-β-geo reporter is observed in the dorsal neural tube at E8.5 (b). At E9.5, OAZ is expressed as two narrow continuous bands along the dorsal midline with the most intense staining in the forebrain, hindbrain and rostral spinal cord (c-dorsal view, d-frontal view). (e-g) X-gal staining in transverse sections of E9.5 $OAZ^{lacZ/+}$ embryo. Stronger X-gal staining is detected at the dorsal neuroepithelium flanking the roof-plate. Rp, roof-plate; Fb, forebrain; Hb, hindbrain. (h) X-gal staining in sagittal section of E14.5 $OAZ^{lacZ/+}$ embryo reveals OAZ expression in the olfactory epithelium (Oe), septum (Spt), thalamus (Th), midbrain (Mb) ventricular zone and the cerebellar primordium (Cb). Weak X-gal staining is also detected in the cortical ventricular zone. (I–k) OAZ expression in the developing cerebellum. In $OAZ^{lacZ/+}$ mice, X-gal staining is detected in the external granular layer (egl) and Purkinje cell layer (pcl). The expression decreases postnatally and is absent in adults. Note stronger staining is observed in rostral lobes than in caudal lobes. Scale bars, 250 μm.

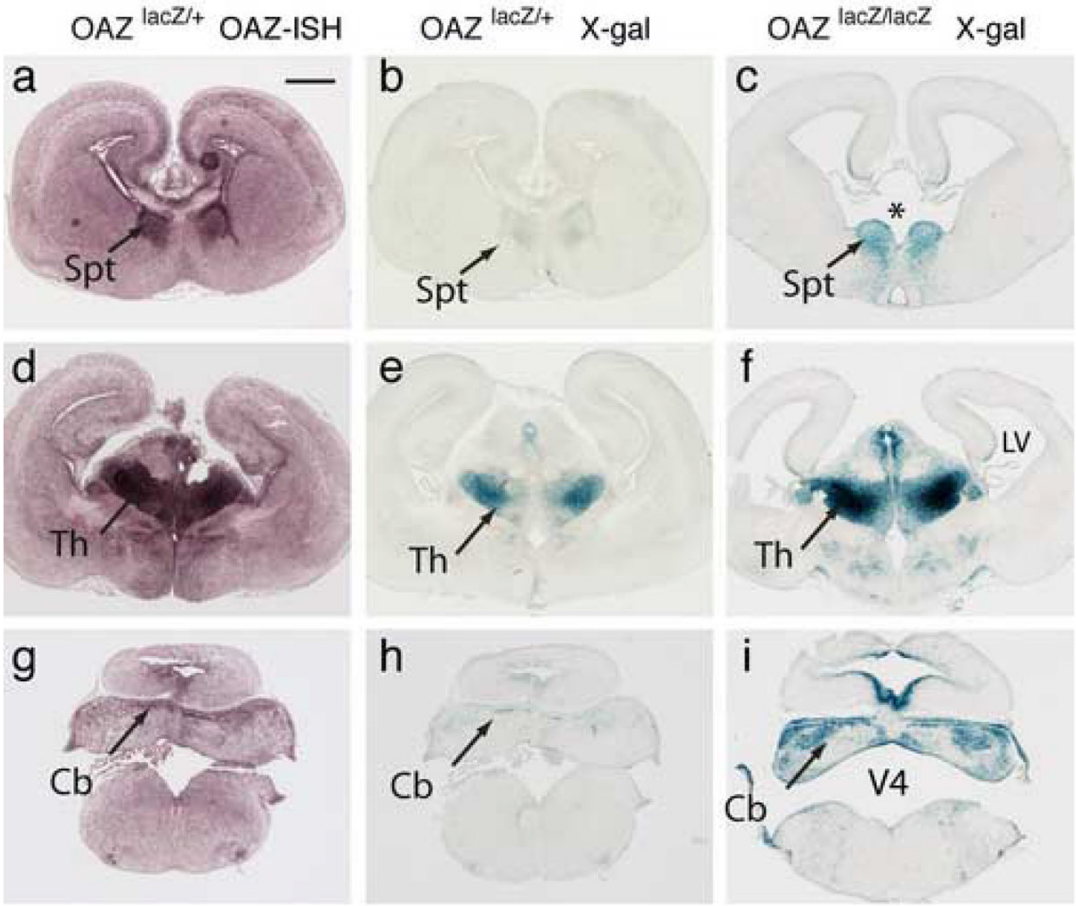

Figure 2.

Early midline defects in homozygous *OAZ*$^{lacZ/lacZ}$ mice at E15.5

(a, d, g) *In situ* hybridization with an *OAZ* probe shows endogenous OAZ expression in the septum (Spt), thalamus (Th) and cerebellum (Cb). (b, e, h) X-gal staining in *OAZ*$^{lacZ/+}$ embryos demonstrates that the pattern of X-gal staining faithfully mimics the endogenous OAZ expression. (c, f, i) X-gal staining in *OAZ*$^{lacZ/lacZ}$ embryos revealed midline defects in the forebrain and hindbrain. At the forebrain (c), the septum is reduced in *OAZ*$^{lacZ/lacZ}$ embryos, and a gap (indicated by "*") is present in the ventral midline area. At the hindbrain (i), the cerebellar plate and the medulla oblongata are considerably smaller, while the fourth ventricle (V4) is enlarged. The lateral ventricles (LV) are also enlarged (c, f). Scale bar: a–i, 500 μm (in a).

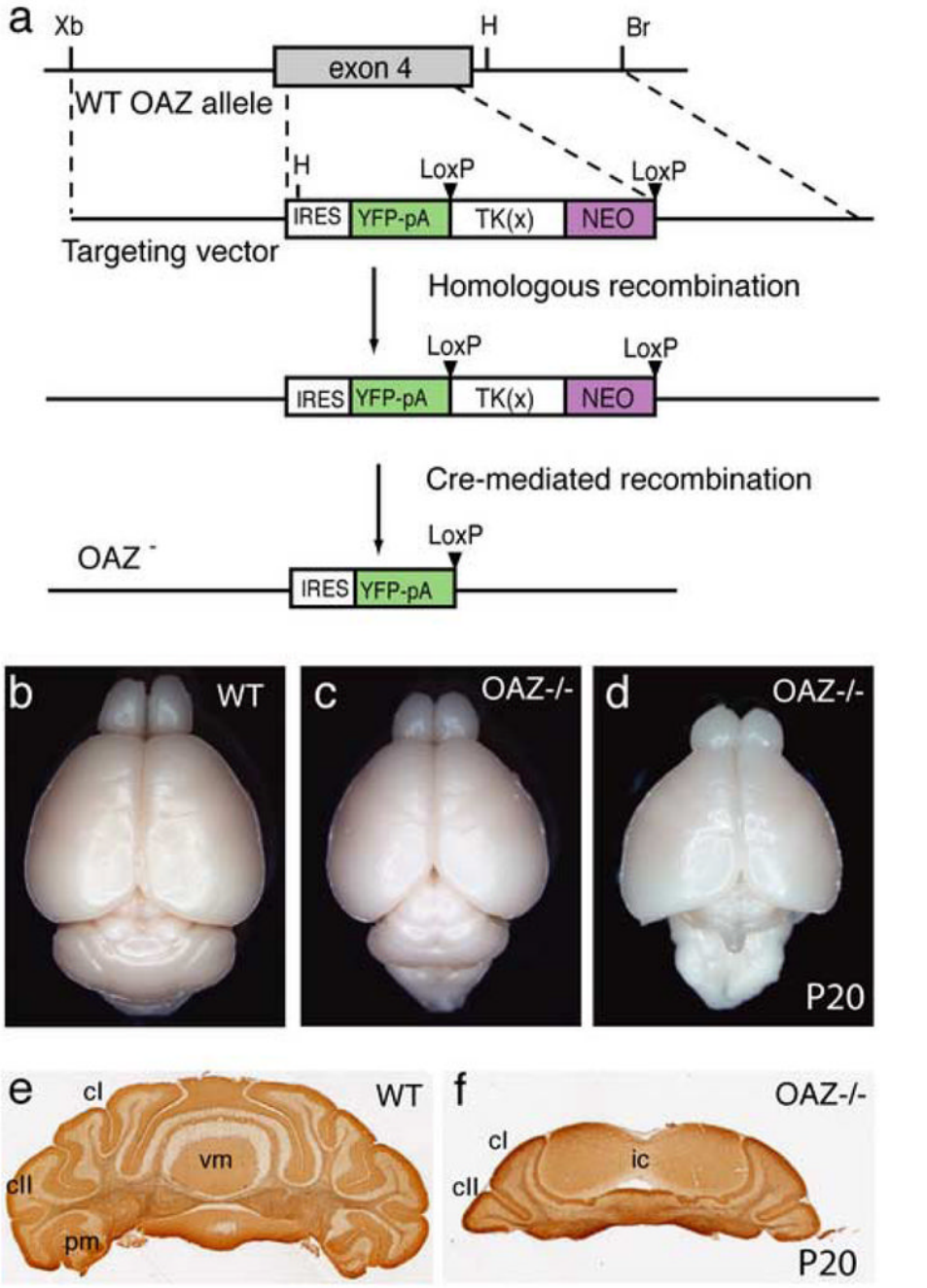

Figure 3.

Targeted deletion of *OAZ* gene and cerebellar anomalies in *OAZ*$^{-/-}$ mice

(a) Schematic representation of *OAZ* gene knock-out allele. The *IRES-YFP-polyA-LTNL* cassette was inserted at amino acid 112 and deleted exon 4. (b–d) Dorsal views of whole-mount brain show the reduction of cerebellum particularly the vermis region in P20 *OAZ*$^{-/-}$ mice. In a more severely affected animal (d), the entire cerebellum is absent. (e, f) Coronal sections through the cerebella confirm the loss of most vermis region in *OAZ*$^{-/-}$ mice. cI, crus I; cII, crus II; pm, paramedian lobule; ic, inferior colliculus.

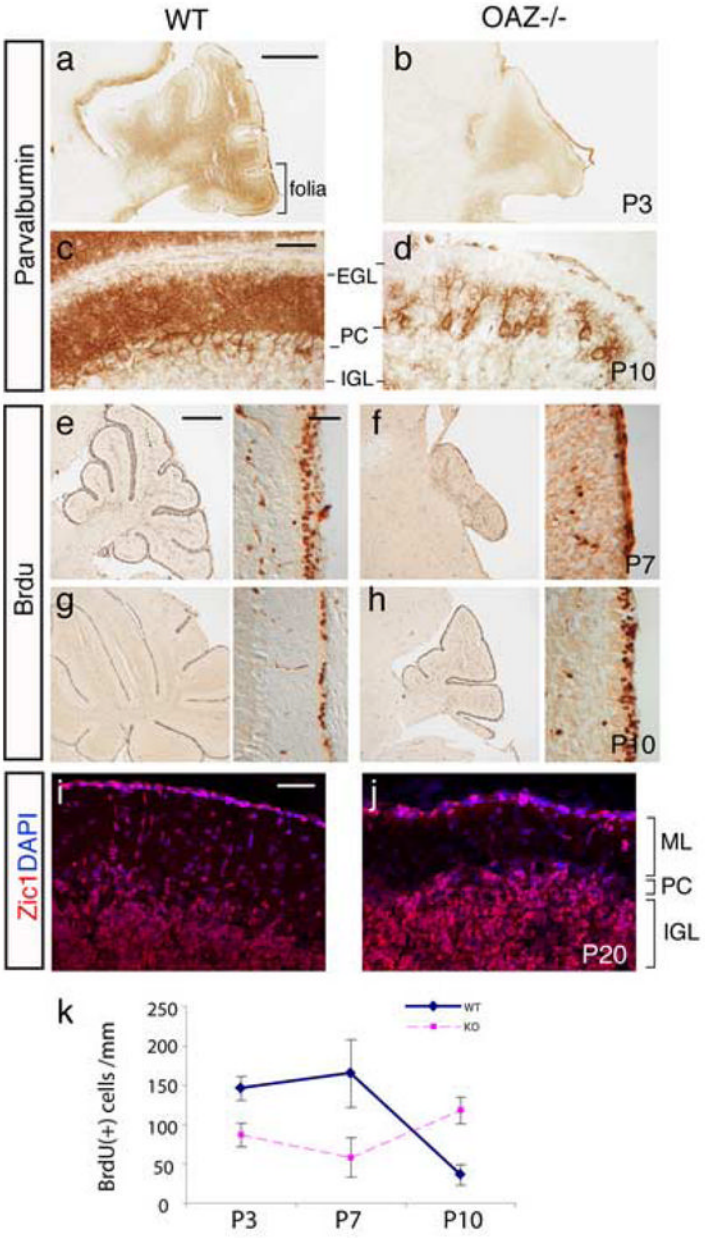

Figure 4.

Characterization of postnatal cerebellar development in *OAZ*$^{-/-}$ mice

(a–d) Defects of PC differentiation in *OAZ*$^{-/-}$ mice. Sagittal sections through cerebella were stained for parvalbumin, a gene highly expressed in PCs. At P3 (a, b), the cerebellar foliation was absent in *OAZ*$^{-/-}$ mice. At P10 (c, d), the number and dendritic arborization of PCs were greatly reduced in *OAZ*$^{-/-}$ mice. (e–h) BrdU-labeling of proliferating GC progenitors at EGL. The *OAZ*$^{-/-}$ mice show a reduced number of BrdU-positive cells at P7, but an increase at P10, indicating a delay of GC proliferation. (i, j) Zic1 staining reveals mature GCs at the internal granular layer (IGL) in adult (P20) *OAZ*$^{-/-}$ mice. ML, molecular layer. (k) Quantification of GC proliferation. Mean and SDs of BrdU-positive cells per 20μm section of cerebellum at P3, P7 and P10, counted from wild-type or *OAZ*$^{-/-}$ brains (n = 3 sections each). The number is

normalized by the length of EGL at each section. Scale bars: a, b, 500 μm (in a); c, d, 50 μm (in c); e–h left panels, 500 μm (in e); right panels, 50 μm (in e); i, j, 50 μm (in i).

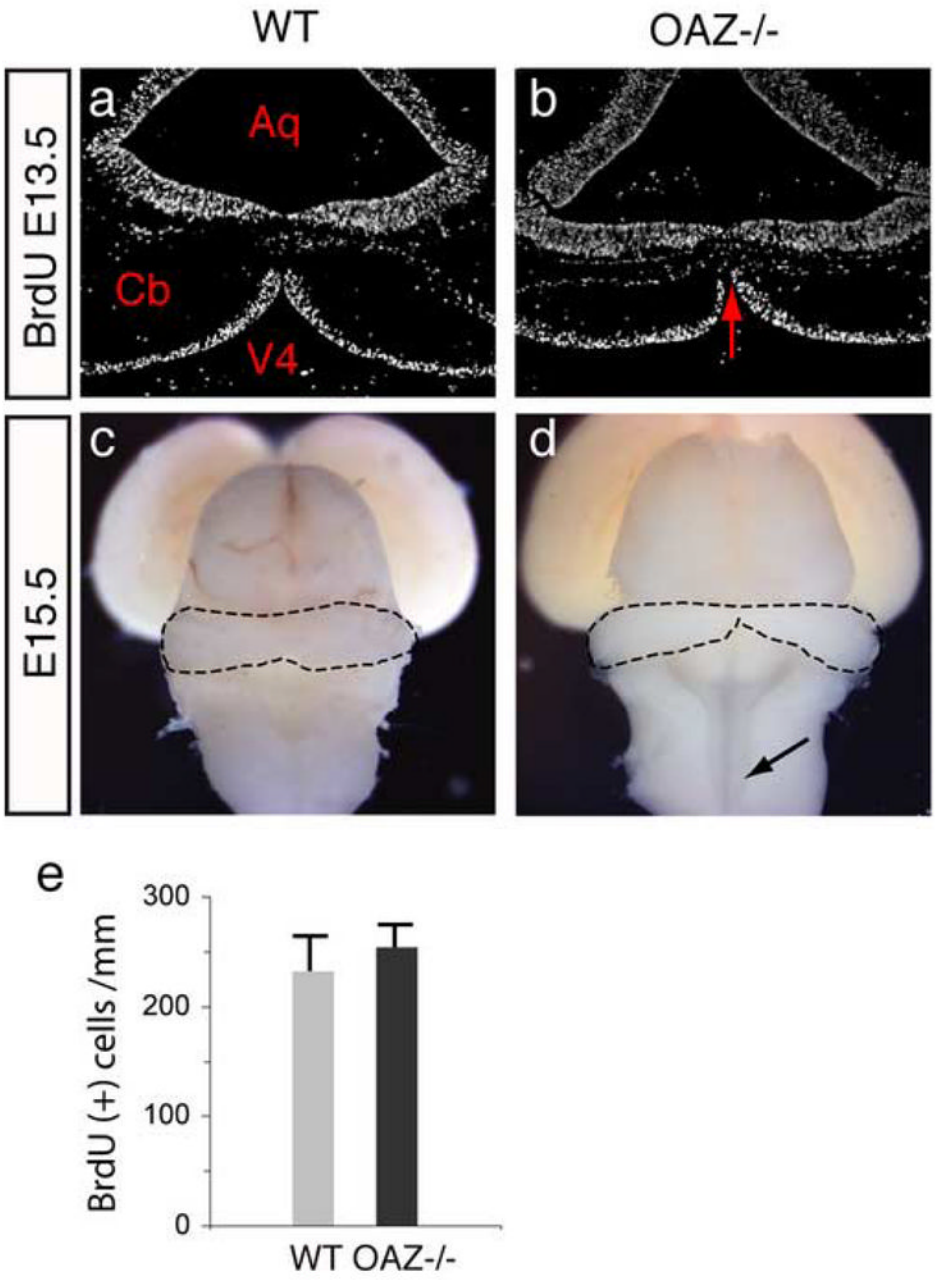

Figure 5.

OAZ loss-of-function affects cerebellar midline fusion

(a, b) BrdU labeling on E13.5 coronal sections. The cerebellar primordia are considerably smaller and the fusion area is limited in $OAZ^{-/-}$ embryos (arrows). The pattern of BrdU labeled cells at the cerebellar ventricular zone appears similar. Aq, aqueduct; V4, fourth ventricle; Cb, cerebellum. (c, d) Dorsal views of E15.5 brain show limited cerebellar fusion in $OAZ^{-/-}$ embryos. In wild-type mice, the two cerebellar primordia fuse at the midline and form a tube structure (dashed line), while in $OAZ^{-/-}$ mice, the two primordia barely attach at the middle and the rostral spinal cord remains open (arrows). (e) Quantification of proliferation at the cerebellar ventricular zone at E13.5.

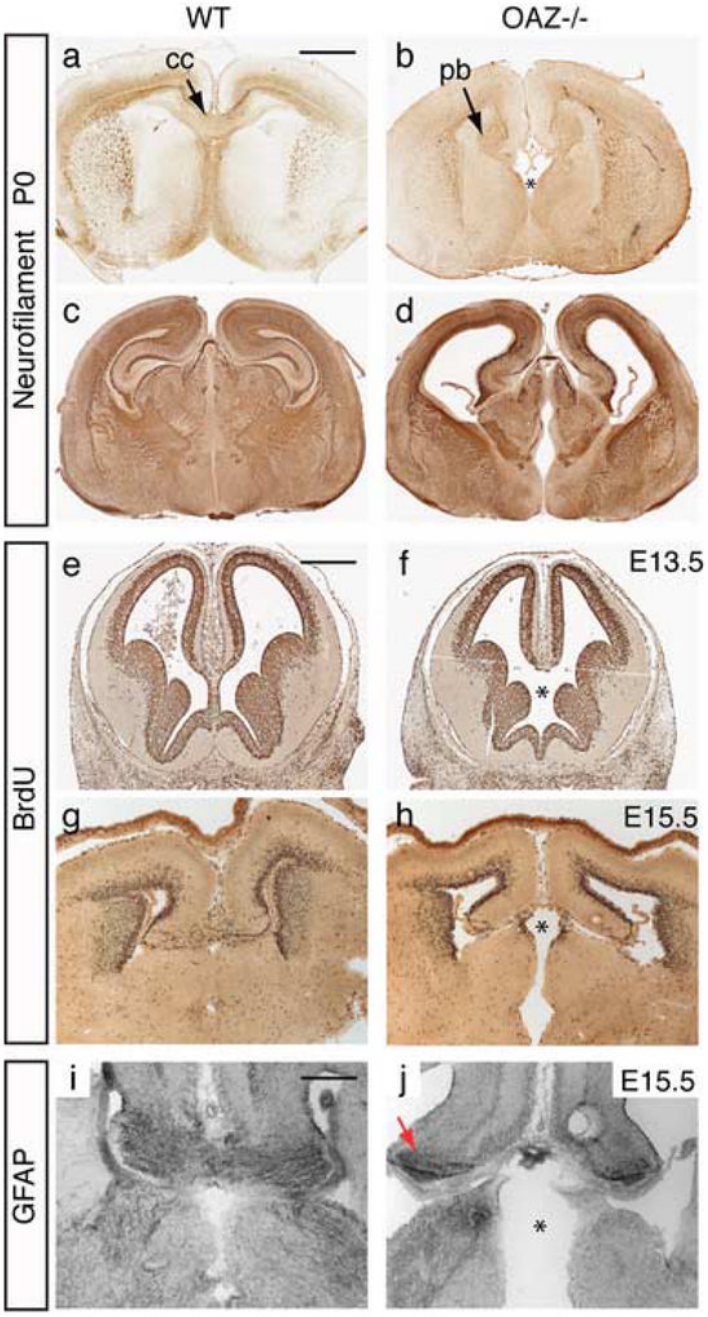

Figure 6.

Forebrain midline defects in *OAZ*$^{-/-}$ mice

(a–d) Neurofilament staining on coronal sections reveals that the corpus callosum (cc) and hippocampal axons fail to cross the midline, and swirl into Probst bundles (pb) in *OAZ*$^{-/-}$ mice. In some mutants (d), an enlargement of the cerebral ventricle is also observed. (e–h) Defects of the forebrain septal region in *OAZ*$^{-/-}$ embryos. At E13.5 and E15.5, BrdU labeling shows normal pattern of proliferating cortical neurons in *OAZ*$^{-/-}$ embryo. Note the septal region is smaller in *OAZ*$^{-/-}$ embryos (indicated by "*"). (i, j) Midline glia distribution was examined using an anti-GFAP antibody. At E15.5, GFAP staining marks the midline glia as a continuous cell stream connecting the two cortical hemispheres at the corticoseptal boundary in wild-type

mice. In *OAZ*$^{-/-}$ mice, GFAP staining remains at the medial cortical edge (arrows), but failed to connect the two hemispheres. Scale bars: a–d, 1000 μm (in a); e–f, 500 μm (in e); i, j, 250 μm (in i).

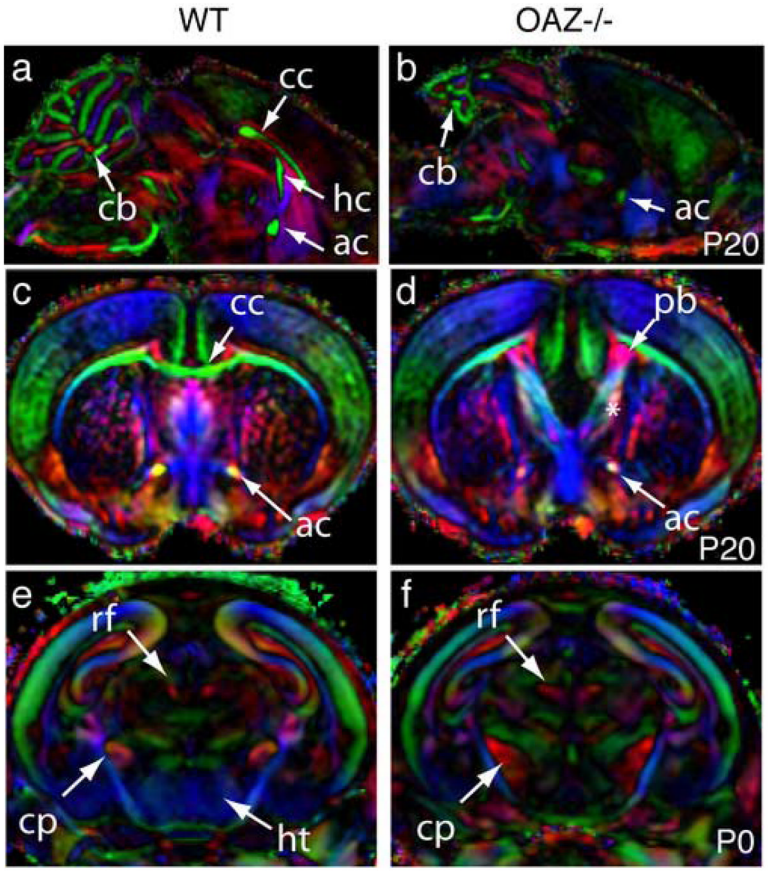

Figure 7.

Diffusion tensor magnetic resonance imaging (μDTI) reveals widespread midline defects in *OAZ*$^{-/-}$ mice

(a, b) Midsagittal plane shows the absence of corpus callosum (cc), hippocampal commissure (hc) and reduction of cerebellum (cb) in *OAZ*$^{-/-}$ brain. (c, d) A coronal plane through the forebrain shows the absence of corpus callosum, the appearance of the Probst bundles (pb), and the abnormal septal region (*) in an *OAZ*$^{-/-}$ brain. The anterior commissure (ac) is present but smaller in *OAZ*$^{-/-}$ mice. (e, f) Coronal plane through the midbrain reveals the reduction of the anterior hypothalamus (ht) and the expansion of cerebral peduncle (cp) and fasciculus retroflexus (rf) in a P0 *OAZ*$^{-/-}$ brain. Axon tract orientation is pseudocolored by the μDTI software: dorsal-ventral (blue), anterior-posterior (red) and left-right (green).

Table 1

Summary of *OAZ* genotype/survival at various ages

Parents	Age genotyped	Number of litters	Genotype		
			+/+	+/−	−/−
$OAZ^{+/-} \times OAZ^{+/-}$	Embryos +neonates	10	26 (28%)	44 (47%)	24(26%)
$OAZ^{+/-} \times OAZ^{+/-}$	2–4 weeks	13	29 (27%)	62 (57%)	17(16%)
$OAZ^{lacZ/+} \times OAZ^{lacZ/+}$	Embryos +neonates	13	29 (25%)	54(46%)	34(29%)
$OAZ^{lacZ/+} \times OAZ^{lacZ/+}$	2–4 weeks	31	61 (36%)	107(63%)	2(1%)
$OAZ^{+/-} \times OAZ^{lacZ/+}$	2–4 weeks	8	36(50%)	34(48%)	2(3%)